Wave spectral shapes in the coastal waters based on measured data off Karwar, west coast of India

Anjali Nair M, Sanil Kumar V

Ocean Engineering Division

Council of Scientific & Industrial Research-National Institute of Oceanography

Dona Paula 403 004, Goa India

*Correspondence to email:sanil@nio.org Tel: 0091 832 2450 327

Abstract

Understanding of the wave spectral shapes is of primary importance for the design of marine facilities. In this paper, the wave spectra collected from January 2011 to December 2015 in the coastal waters of the eastern Arabian Sea using the moored directional waverider buoy are examined to know the temporal variations in the wave spectral shape. Over an annual cycle, for 31.15% of the time, peak frequency is between 0.08 and 0.10 Hz and the significant wave height is also relatively high (~ 1.55 m) for waves in this class. The slope of the high-frequency tail of the monthly average wave spectra is high during the Indian summer monsoon period (June-September) compared to other months and it increases with increase in significant wave height. There is not much interannual variation in slope for swell dominated spectra during the monsoon, while in the non-monsoon period, when wind-seas have much influence, the slope varies significantly. Since the exponent of the high-frequency part of the wave spectrum is within the range from -4 to -3 during the monsoon period, Donelan spectrum shows better fit for the high-frequency part of the wave spectra in monsoon months compared to other months.

Key Words: Ocean surface waves, wind waves, Arabian Sea, wave spectrum, high-frequency tail

1. Introduction

Information on wave spectral shapes are required for designing marine structures (Chakrabarti, 2005) and almost all the wave parameters computations are based on the wave spectral function (Yuan and Huang, 2012). The growth of waves and the correspondent spectral shape is due to the complex ocean-atmosphere interactions, while the physics of air-sea interaction is not completely understood (Cavaleri et al., 2012). The shape of the wave spectrum depends on the factors governing the wave growth and decay, and a number of spectral shapes have been proposed in the past for different sea states (see Chakrabarti, 2005 for a review). The spectral shape is maintained by nonlinear transfer of energy through nonlinear four-wave interactions (quadruplet interactions) and white-capping (Gunson and Symonds, 2014). The momentum flux between the ocean and atmosphere govern the high-frequency wave components (Cavaleri et al., 2012). According to Philips, the equilibrium ranges for low-frequency and high-frequency region is proportional to f^{-5} and f^{-4} (where f is the frequency) respectively. Several field studies made since JONSWAP (Joint North Sea Wave Project) field campaign reveals an analytical form for wave spectra with the spectral tail proportional to f^{-4} (Toba, 1973; Kawai et al., 1977; Kahma, 1981; Forristall, 1981; Donelan et al., 1985). Usually, there is a predominance of swell fields in large oceanic areas, which is due to remote storms (Chen et al., 2002; Hwang et al., 2011; Semedo et al., 2011). The exponent used in the expression for the frequency tail has different values (see Siadatmousavi et al., 2012 for a brief review). For shallow water, Kitaigordskii et al. (1975) suggested f^{-3} tail, Liu (1989) suggested f^{-4} for growing young wind-seas and f^{-3} for fully developed wave spectra. Badulin et al. (2007) suggested f^{-4} for frequencies where nonlinear interactions are dominant. The study carried out at Lake George by Young and Babanin (2006) revealed that in the frequency range $5f_p < f < 10f_p$, the average value of the exponent 'n' of f^{-n} is close to 4. Whereas, some studies in real sea conditions indicate that high-frequency shape of f^{-4} applies up to few times the peak frequency (f_p) and then decays faster with frequency. The spectra for coastlines in Currituck Sound with short fetch condition showed a decay closer to f^{-5} when f is greater than two or three times the peak frequency (Long and Resio, 2007). Gagnaire-Renou et al. (2010) found that the energy input from wind and dissipation due to white-capping have a significant influence on the high-frequency tail of the spectrum.

The physical processes in the north Indian Ocean have a distinct seasonal cycle (Shetye et al., 1985; Ranjha et al., 2015) and the surface wind-wave field is no exception (Sanil Kumar et al., 2012). In the eastern Arabian Sea (AS), significant wave height (H_{m0}) up to 6 m is measured in the monsoon period (June to September), and during rest of the period, H_{m0} is normally less than 1.5 m (Sanil Kumar and Anand, 2004). Sanil Kumar et al. (2014) observed that in the eastern AS, the wave spectral shapes are different at two locations within 350 km distance, even though the difference in the integrated parameter like H_{m0} is marginal. Dora and Sanil Kumar (2015) observed that waves at 7-m water depth in the nearshore zone off Karwar are high energy waves in the monsoon and low to moderate waves in the non-monsoon period (January to May and October to December). Dora and Sanil Kumar (2015) study shows similar contribution of wind-seas and swells during the pre-monsoon (February to May), while swells dominate the wind-sea in the post-monsoon (October to January) and the monsoon period. A study was carried out by Glejin et al. (2012) to find the variation in wave characteristics along the eastern AS and the influence of swells in the nearshore waves at 3 locations during the monsoon period in 2010. This study shows that the percentage of swells in the measured waves was 75% at the southern part of AS and 79% at the northern part of AS. Wind and wave data measured at a few locations along the west coast of India for short-period, one to two months as well as the wave model results were analysed to study the wave characteristics in the deep as well as nearshore regions during different seasons (Vethamony et al., 2013). From the wave data collected for two years period (2011 and 2012) along the eastern AS, the swells of period more than 18 s and significant wave height less than 1 m which occur for 1.4 to 3.6% of the time were separated and their characteristics were studied by Glejin et al. (2016). Anjali Nair and Sanil Kumar (2016) presented the daily, monthly, seasonal and annual variations in the wave spectral characteristics for a location in the eastern AS and reported that over an annual cycle, 29 % of the wave spectra are single-peaked spectra and 71 % are multi-peaked spectra. Recently Amrutha et al. (2017) by analysing the measured wave data in October reported that the high waves (significant wave height > 4 m) generated in an area bounded by 40-60° S and 20-40° E in the south Indian Ocean reached the eastern AS in 5-6 days and resulted in the long-period waves. The earlier studies indicate that the spectral tail of the high-frequency part shows large variation and its variation with seasons are not known. Similarly, the shape of the parametric spectra are also different and hence it is important to identify the spectral shapes based on the measured data covering all the seasons and different years.

The discussion above shows that there is a strong inspiration to study the high-frequency tail of the wave spectrum. For the present study, we used the directional waverider buoy measured wave spectral data at 15-m water depth off Karwar, west coast of India, over 5 years during 2011 to 2015 and evaluated the nearshore wave spectral shapes in different months. This study addresses two main questions: (1) How the high-frequency tail of the wave spectrum varies in different months, and (2) What are the spectral parameters for the best-fit theoretical spectra. This paper is organized as follows: the study area is introduced in section 2, details of data used and methodology in section 3. Section 4 presents the results of the study and the conclusions are given in section 5.

2. Study area

The coastline at Karwar is 24º inclined to the west from the north, and the 20 m depth contour is inclined 29º to the west. Hence, large waves in the nearshore will have an incoming direction close to 241º, since waves get aligned with the depth contour due to refraction. At 10, 30 and 75 km distance from Karwar, the depth contours of 20, 50 and 100 m are present (Fig. 1). The study region is under the seasonally reversing monsoon winds, with winds from the northeast during the post-monsoon and from the southwest during the monsoon period. The monsoon winds are strong and the total seasonal rainfall is 280 cm. There is a 0.24 m annual cycle in mean sea level from September to January. The average tidal range is 1.58 m during spring tides and 0.72 m during neap tides (Sanil Kumar et al., 2012).

3. Data and methods

The waves off Karwar (14° 49’ 56” N and 74° 6’ 4” E) were measured using the directional waverider buoy (DWR-MKIII) . Measurements are carried out from 1 January 2011 to 31 December 2015. The data of heave and two translational motion of the buoy are sampled at 3.84 Hz. A digital high-pass filter with a cut off at 30 s is applied to the 3.84 Hz samples. At the same time it converts the sampling rate to 1.28 Hz and stores the time series data at 1.28 Hz. From the time series data for 200s, the wave spectrum is obtained through a fast Fourier transform (FFT). During half an hour 8 wave spectra of a 200 s data interval each are collected and averaged to get a representative wave spectrum for half an hour (Datawell, 2009). The wave spectrum is with a

resolution of 0.005 Hz from 0.025 Hz to 0.1 Hz and is 0.01 Hz from 0.1 to 0.58 Hz. Bulk wave parameters; significant wave height (H_{m0}) which equals $4\sqrt{m_o}$ and mean wave period (T_{m02}) based on second order moment, which equals $\sqrt{m_0/m_2}$) are obtained from the spectral moments. Where m_n is the n^{th} order spectral moment ($m_n = \int_0^\infty f^n S(f)df$, n=0 and 2), S(f) is the spectral energy density and f is the frequency. The spectral peak period (Tp) is estimated from the wave spectrum and the peak wave direction (Dp) is estimated based on circular moments (Kuik et al., 1988). The wind-seas and swells are separated through the method described by Portilla et al. (2009) and the wind-sea and the swell parameters are computed by integrating over the respective spectral parts. Measurements reported here are in Coordinated Universal Time (UTC), which is 05:30 h behind the local time. U_{10} is the wind speed at 10-m height obtained from reanalysis data of zonal and meridional components at 6 hourly intervals from NCEP / NCAR (Kalnay et.al., 1996) and is used to study the influence of wind speed on the spectral shape.

Since the frequency bins over which the wave spectrum estimated is same in all years, the monthly and seasonally averaged wave spectrum is computed by taking the average of the spectral energy density at the respective frequencies of each spectrum over the specified time.

Wave spectrum continues to develop through non-linear wave-wave interactions even for very long times and distances. Hence, most of the wave spectrum is not fully developed and cannot be represented by Pierson-Moskowitz (PM) spectrum (Pierson and Moskowitz, 1964). Accordingly, an additional factor was added to the PM spectrum in order to improve the fit to the measured spectrum. The JONSWAP spectrum (Hasselmann et al., 1973) is thus a PM spectrum multiplied by an extra peak enhancement factor γ. The high-frequency tail of the JONSWAP spectrum decays in a form proportional to $f^{-5.}$ A number of studies reported that high-frequency decay is by a form proportional to $f^{-4.}$ Modified JONSWAP spectrum including Toba's formulation of saturation range was proposed by Donelan et al. (1985). The JONSWAP and Donelan spectrum used in the study are given in eqns. (1) and (2).

$$S(f) = \frac{\alpha g^2}{(2\pi)^4 f^5} \exp\left[-\frac{5}{4}\left(\frac{f}{f_p}\right)^{-4}\right] \gamma^{\exp\left[-(f-f_p)^2 / 2\sigma^2 f_p\right]} \quad \text{..... (1)}$$

$$S(f) = \frac{\alpha g^2}{(2\pi)^4 f^4 f_p} \exp\left[-\left(\frac{f}{f_p}\right)^{-4}\right] \gamma^{\exp\left[-(f-f_p)^2 / 2\sigma^2 f_p^2\right]} \quad \text{.....(2)}$$

Where γ is the peak enhancement parameter; α is Philip's constant; f is the wave frequency; g is the gravitational acceleration and σ is the width parameter.

$$\sigma = \begin{cases} 0.07, & f < f_p \\ 0.09, & f \geq f_p \end{cases}$$

An exponential curve $y = kf^b$ is fitted for high-frequency part of the spectrum and the exponent (value of b) and the coefficient k is estimated for the best fitting curve based on statistical measures such as least square error and bias. The slope of the high-frequency part of the wave spectrum is represented by the exponent of the high-frequency tail.

For the present study, JONSWAP spectrum is tested by fitting for the whole frequency range of the measured wave spectrum. It is found out that the JONSWAP spectra do not show a good fit for higher frequency range, whereas Donelan spectrum shows better fit for the high-frequency range. Hence, JONSWAP spectrum is used for the lower frequency range up to spectral peak and Donelan spectrum is used for the higher frequency range from the spectral peak for single-peaked wave spectrum. Theoretical wave spectra are not fitted to the double-peaked wave spectra.

4. Results and discussions

4.1 Bulk wave parameters

Mostly the wave conditions (~ 75%) at the buoy location are intermediate and shallow-water waves (where water depth is less than half the wavelength, $d < L/2$), this condition is not satisfied during ~ 25% of the time due to waves with mean periods of 4.4 s or less. This study, therefore, deals with shallow, intermediate and deepwater wave climatology. Hence, bathymetry will significantly influence the wave characteristics.

181 The persistent monsoon winds generate choppy seas with average wave heights of 2 m and
182 mean wave period of 6.5 s. Fig. 2 shows that in the monsoon, the observed waves had a maximum
183 H_{m0} of about 5 m, with H_{m0} of 2-2.5 m more common during this period. The maximum H_{m0}
184 measured during the study period is on 21 June 2015 17:30 UTC (Fig. 2a). Mean wave periods
185 (T_{m02}) at the measurement location ranged from 4-8 s (Fig. 2b). Wave direction during monsoon is
186 predominantly from the west due to refraction towards the coast. The fluctuation in H_{mo} due to the
187 southwest monsoon is seen in all the years (Fig. 2a). High waves (H_{m0} > 2 m) during 27-29
188 November 2011 are due to the deep depression ARB04 formed in the AS. During the study period,
189 the annual average H_{m0} is same (~1.1 m) in all the years (Table 1). In 2013, the data during August
190 could not be collected and hence resulted in lower annual average H_{m0}. Over the 5 years, small
191 waves (H_{m0} < 1 m) account for a large proportion (63.94%) of measured data and only during
192 0.16% of the time, H_{m0} exceeded 4 m (Table 2). The 25th and 75th percentiles of the H_{m0} distribution
193 over the entire analysis period are 0.6 and 1.4 m.
194
195 Waves with low heights (H_{m0} < 1 m) are with the mean period in a large range (2.7-10.5 s),
196 whereas high waves (H_{m0} > 3m) have mean wave period in a narrow range (6.1-9.3 s) (Table 2).
197 For waves with H_{m0} higher than 3 m, the Tp never exceeded 14.3 s and for waves with H_{m0} less
198 than 1 m, Tp up to 22.2 s are observed (Fig. 2c) and the long period swells (14-20 s) are with H_{m0} <
199 2.5 m. Around 7% of the time during 2011-2015, waves have peak period more than 16.7 s (Table
200 3). Peak frequencies between 0.08 and 0.10 Hz, equivalent to a peak wave period of 10 - 12.5 s are
201 observed 31.15% of the time and the H_{m0} is also relatively high (~ 1.55 m) for waves in this class.
202 During the annual cycle, the wave climate is dominated by low (0.5 > H_{m0} >1m) intermediate-
203 period (Tp ~10-16s) south-westerly swell. Waves from the northwest are with Tp less than 8 s (Fig.
204 3).
205
206 The wave roses during 2011-2015 indicate that around 38% of the time during the period
207 2011 to 2015, the predominant wave direction is SSW (225°) with long period (14 - 18s) and
208 intermediate period (10 - 14s) waves (Fig. 3). A small percentage of long-period waves having H_{m0}
209 more than 1m are observed from the same direction in which more than 80% are swells (Fig. 3c).
210 Intermediate period waves observed having H_{m0} less than 1m, contain 20 - 60% of swells. Around
211 10-15% of the waves observed during the period are from the west, which includes intermediate
212 and short period waves with H_{m0} varying from 1.5 to 3m. These intermediate period waves from

west having H_{m0} between 2.5 - 3m contain more than 80% of swells. Waves from NW are short period waves with H_{m0} between 0.5 and 1.5; in which swell percentage is very less showing the influence of wind-sea (Fig. 3d). High waves observed in the study area consists of more than 80% swells.

Date versus year plots of significant wave height (Fig. 4) shows that H_{m0} has its maximum values (H_{m0} >3m) during the monsoon period with a wave direction of WSW and peak wave period of 10 - 12s (intermediate period). The mean wave period shows its maximum values (6 - 8s) during the monsoon period. During January–May in all the years, H_{m0} is low (H_{m0} < 1m) with waves from SW, W and NW directions. NW waves observed are the result of strong sea breezes existing during this period. Both long-period (Tp > 14s), intermediate-period (10 < Tp <14s) and short-period (Tp < 8s) waves are observed during this period and hence, the mean wave period observed is low compared to the monsoon (Fig. 4d). During October to December, similar to the pre-monsoon period, H_{m0} observed is less than 1m, but the wave direction is predominantly from SW and W, with least NW waves. Short period waves are almost absent during this period, and the condition is similar for all the years. The interannual variations in H_{m0} are less than 15% (Fig. 4). Primary seasonal variability in waves is due to the monsoonal wind reversal. During January-March, there is a shift in the occurrences of northwest swells.

4.2 Wave spectrum

The normalized wave spectral energy density contours are presented for different years to know the wind-sea/swell predominance (Fig. 5). Normalisation of the wave spectrum is done to know the spread of energy in different frequencies. Since the range of maximum spectral energy density in a year is large (~ 60 m^2/Hz), each wave spectrum is normalised through dividing the spectral energy density by the maximum spectral energy density of that spectrum. The predominance of both the wind-seas and swells are observed in the non-monsoon period, whereas in the monsoon only swells are predominant (Fig. 5). The separation of swells and wind-seas indicates that over an annual cycle, around 54% of the waves are swells. Glejin et al. (2012) reported that the dominance of swells during monsoon is due to the fact that even though the wind at the study region is strong during monsoon, the wind over the entire AS also will be strong and when these swells are added to the wave system at the buoy location, the energy of the swell increases (Donelan, 1987) and will result in dominance of swells. The spread of spectral energy to

246 higher frequencies (0.15 to 0.25 Hz) is predominant during January-May (Fig. 5) due to sea-breeze
247 in the pre-monsoon period (Neetu et al., 2006; Dora and Sanil Kumar, 2015). In the monsoon
248 during the wave growth period, the spectral peak shifts from 0.12-0.13 Hz to 0.07-0.09 Hz (lower
249 frequencies).
250
251 An interesting phenomenon is that the long-period (> 18 s) swells are present for 2.5% of
252 the time during the study period. The buoy location at 15 m water depth is exposed to waves from
253 northwest to south with the nearest landmass at ~ 1500 km in the northwest (Asia), ~ 2500 km in
254 the west (Africa), ~ 4000 km in the southwest (Africa) and ~ 9000 km in the south (Antarctica)
255 (Amrutha et al., 2017). Due to its exposure to the Southern Oceans and the large fetch available,
256 swells are present all year round in the study area and the swells are dominant in the non-monsoon
257 (Glejin et al., 2013). Throughout the year, waves with period more than 10 s (low-frequency < 0.1
258 Hz waves) are the southwest swells whereas with seasons the direction of short-period waves
259 changes (Fig. 5). Amrutha et al. (2017) reported that the long-period waves observed in the eastern
260 AS are the swells generated in the south Indian Ocean. In the monsoon season, the waves with
261 high-frequency are predominantly from west-southwest, whereas in the non-monsoon they are from
262 the northwest. In the non-monsoon period, the predominance of wind-seas and swells fluctuated
263 and hence the mean wave direction also changed frequently (Fig. 5). The average direction of
264 waves with H_{m0} < 1m shows the northwest wind-seas and the southwest swells, whereas, for high
265 waves (H_{m0} > 3m), the difference between the swell and wind-sea direction decreases. This is
266 because the high waves get aligned to the bottom contour before 15 m water depth on its approach
267 to the shallow water.
268
269 The interannual changes of wave spectral energy density for different months in the period
270 2011-2015 are studied by computing the monthly average wave spectra for all the years (Fig. 6). In
271 the non-monsoon period, the wave spectra observed is double-peaked, indicating the presence of
272 wind-seas and swells, whereas during the monsoon, due to the strong southwest winds, single
273 peaked spectrum is observed, i.e. the swell peak with low-frequency and high spectral energy
274 density. Along the Indian coast, Harish and Baba (1986), Rao and Baba (1996) and Sanil Kumar et
275 al. (2003) found out that wave spectra are generally multipeaked and that the double peaked wave
276 spectra are more frequent during low-sea states (Sanil Kumar et al., 2004). Sanil Kumar et al.
277 (2014), Sanil Kumar and Anjali (2015) and Anjali and Sanil Kumar (2016) have also observed that

double-peaked spectrum in the monsoon period in the eastern AS are due to the locally generated wind-seas and the south Indian Ocean swells. In the study area, from January to May and October to December, the swell peak is between the frequencies 0.07 and 0.08 Hz ($12.5 < Tp < 14.3$s), but in the monsoon period, the swell peak is around 0.10 Hz, in all the years studied. This shows long-period swells ($Tp > 13$s) in the non-monsoon period and intermediate period swells ($8 < Tp < 13$s) in the monsoon. Glejin et al. (2016), also observed the presence of low-amplitude long-period waves in the eastern AS in the non-monsoon period and intermediate period waves in the monsoon period. This is because of the propagation of swells from the southern hemisphere is more visible during the non-monsoon period due to the calm conditions (low wind-seas) prevailing in the eastern AS. Whereas during the monsoon period, these swells are less due to the turbulence in the north Indian Ocean (Glejin et al., 2013). Large interannual variations are observed for monthly average wave spectrum in all months except in July. This is because July is known to be the roughest month over the entire annual cycle and southwest monsoon reaches its peak during July. Hence, the influence of temporally varying wind-seas on the wave spectrum is least during July compared to other months. Due to the early onset (on 1 June) and advancement of monsoon during 2013 compared to other years, the monthly average value of the maximum spectral energy is observed in June 2013 (Fig. 6). The wave spectra of November 2011 is distinct from that of other years, with low wind-sea peak frequency, i.e. 0.13 Hz due to the deep depression ARB04, occurred south of India near Cape Comorin, during 26 November–1 December, with a sustained wind speed of 55 km/h. During October 2014, the second peak is observed at 0.11 Hz with comparatively high energy showing the influence of cyclonic storm NILOFAR. It is an extremely severe cyclonic storm that occurred during the period 25-31 October 2014, originated from a low-pressure area between Indian and Arabian Peninsula, with the highest wind speed of 215 km/h and affected the areas of India, Pakistan and Oman. Significant interannual variation is observed in the wind-sea peak frequency. Wave spectra averaged over each season (Fig. 7) shows that the interannual variations in energy spectra averaged over full year period almost follows the pattern of wave spectra averaged over monsoon period, indicating the strong influence of monsoon winds over the wave energy spectra in the study area. Interannual variations within the spectrum are more for wind-sea region compared to swell region. During the study period, the maximum spectral energy observed is during 2011 monsoon.

For different frequencies, the monthly average wave direction is shown in Fig. 8. It is observed that throughout the year the mean wave direction of the swell peak is southwest (200-250^{o}). In the non-monsoon period, the wind-sea direction is northwest (280-300°), except in October and November. This is due to the wind-seas produced by sea breeze which has the maximum intensity during the pre–monsoon season. Interannual variability in wave direction is highest during October and November, where the wind-seas from southwest direction are also observed. This is because, during these months, the wind speed and the strength of the monsoon swell decreases, which makes the low energy wind-seas produced by the withdrawing monsoon winds more visible.

Contour plots of spectral energy density (normalized) clearly show the predominance of wind-seas and swells during the non-monsoon period (Fig. 9). Only Figs. 5 and 9 present the normalised spectral energy density. In the monsoon period, the spectral energy density is mainly confined to a narrow frequency range (0.07-0.14 Hz) and the wave spectra are mainly single peaked with maximum energy within the frequency range 0.08-0.10 Hz, having direction 240^{o}. Glejin et al. (2012) reported that in the monsoon season, the spectral peak is between 0.08 and 0.10 Hz (12-10s) for ~ 72% of the time in the eastern AS. Earlier studies also reported dominance of swells in the eastern AS during the monsoon (Sanil Kumar et al., 2012; Glejin et al., 2012). Above 0.15 Hz, energy gradually decreases, with the lowest energy observed between 0.30 and 0.50 Hz. Wind-sea energy is comparatively low during October, November and December and occurs mostly in the frequency range less than 0.20 Hz, whereas, during January-May, the frequency exceeds 0.20 Hz. In the pre-monsoon period, wind-sea plays a major role in nearshore wave environment (Rao and Baba, 1996). Wind-sea energy is found to be low during April 2015 (Fig. 6), because of reduction in local winds. The occurrence of wind-seas is very less during most of the time in November except during 2011, due to the deep depression ARB04.

.

The behavior of the high-frequency part of the spectrum is governed by the energy balance of waves generated by the local wind fields. When the wind blows over a long fetch or for a long time, the wave energy for a given frequency reaches the equilibrium range and the energy input from the wind is balanced by energy loss to lower frequencies and by wave breaking (Torsethaugen and Haver, 2004). The high-frequency tail slope of the monthly average wave spectrum in different years shows that the slope is high ($b < -3.1$), during June to September and the case is same for all

341 the years studied (Table 4). During all other months, the exponent in the expression for the
342 frequency tail is within the range - 3.1 to -1.5. The distribution of exponent values for different
343 significant wave height ranges shows that the slope increases (exponent decrease from -2.44 to -
344 4.20) as the significant wave height increases and reaches a saturation range. For frequencies from
345 0.23 to 0.58 Hz in the eastern AS during January-May, Amrutha et al. (2017) observed that the
346 high-frequency tail has $f^{-2.5}$ pattern at 15 m water depth and for frequencies ranging from 0.31 to
347 0.55 Hz, the high-frequency tail follows f^{-3} at 5 m water depth. Since H_{mo} is maximum during the
348 monsoon period, the slope is also maximum during June to September. There is no much
349 interannual variation in slope for swell dominated spectra during the monsoon, while in the non-
350 monsoon period when wind-seas have much influence, the slope varies significantly.
351
352 The most obvious manifestations of nonlinearity are sharpening of the wave crests and the
353 flattening of the wave troughs and these effects are reflected in the skewness of the sea surface
354 elevation (Toffoli, 2006). Zero skewness indicates linear sea states, positive skewness value
355 indicate that the wave crests are bigger than the troughs. Figure 10 shows that nonlinearity
356 increases with increase in H_{m0}. The slope of the high-frequency end of the wave spectrum becomes
357 steeper when the wave nonlinearity increases. Donelan et al. (2012) find that in addition to the k^{-4}
358 dissipation that swells modulate the equilibrium in breaking waves dependent on the mean surface
359 slope, while Melville (1994) also quantified a relation between wave packet slopes and dissipation
360 rate. These results are specific to breaking waves, but one might expect similar relations between
361 surface dynamics and dissipation rate for non breaking waves. A function of the form: $A * \exp(\lambda$
362 $H_{m0}) + s0$, with initial parameters of $A = 8$, $\lambda = -2.4$, $s0 = -3.7$ is found to fit the exponent of the
363 high-frequency tail data with the significant wave height (Fig. 11a). The functional representation
364 of the exponent of the high-frequency tail data with H_{m0} shown in Fig. 11a might be useful in
365 revealing the physical connection, and at the very least would provide a predictive basis relating
366 spectral slopes with mean significant wave heights as a basis for future research. It is shown in Fig.
367 11b that the exponent decreases (slope increases) as the mean wave period increases. The study
368 shows that the tail of the spectrum is influenced by the local wind conditions (Fig. 11c) and the
369 influence is more with the zonal component (u) of the wind than on the meridional component (v)
370 (Figs. 11e and 11f). The exponent of the high-frequency tail decreases with the increase of the
371 inverse wave age (U_{10}/c), where c is the celerity of the wave.
372

373 4.3 Comparison with theoretical wave spectra
374
375 In the monsoon period, the spectrum is single peaked with high spectral energy density and
376 during this period JONSWAP spectrum is fitted up to the peak frequency and after that Donelan
377 spectrum is used. The monthly average wave spectra during the monsoon period for the year 2011,
378 is compared with JONSWAP and Donelan theoretical wave spectra in Figure 12. It is found that
379 JONSWAP and Donelan spectra with modified parameters describe well the wave spectra at low
380 frequencies and high frequencies respectively. The values for α and Υ were varied from 0.0001 to
381 0.005 and 1.1 to 3.3 respectively to find out the values for which, the theoretical spectrum best fits
382 the measured spectrum and those values were used to plot the theoretical spectrum. The values of α
383 and Υ thus obtained, for June, July, August and September are given in Table 6. From the table, the
384 average values of α and Υ, for the monsoon months are obtained as 0.0009 and 1.82 for JONSWAP
385 spectra and 0.0274 and 1.64 for Donelan spectra respectively. These values are less than the
386 generally recommended values of α and Υ; 0.0081 and 3.3. α is a constant that is related to the
387 wind speed and fetch length. For all the data, Donelan spectrum fitted is proportional to f^{-n}, where n
388 is the exponent value of the high-frequency tail. The theoretical spectrum JONSWAP and Donelan
389 cannot completely describe the high-frequency tail of the measured spectrum since the high-
390 frequency tail in these spectrum decays in the form of f^{-5} and f^{-4} respectively. Since the exponent of
391 the high-frequency tail of the wave spectrum is within the range -4 to -3 during the monsoon
392 period, Donelan spectrum shows better fit for monsoon spectra compared to other months (Fig.
393 11).
394
395 **5. Concluding remarks**
396
397 In this paper, the variations in the wave spectral shapes in different months for a nearshore
398 location are investigated, based on in situ wave data obtained from a moored directional waverider
399 buoy. Interannual variations within the spectrum are more for wind-seas compared to swells. The
400 maximum significant wave height measured at 15 m water depth is 5 m and the annual average H_{m0}
401 has similar value (~1.1 m) in all the years. Over the 5 years, small waves ($H_{m0} < 1$ m) account for a
402 large proportion of measured data (63.94% of the time). The study shows that high waves ($H_{m0} > 2$
403 m) are with spectral peak period between 8 and 14 s and the long period swells (14-20 s) are with
404 $H_{m0} < 2.5$ m. The high-frequency slope of the wave spectrum (the exponent decreases from -2.44 to

-4.20) increases with increase in significant wave height and mean wave period. During the monsoon period, Donelan spectrum shows better fit for monsoon spectra compared to other months since the exponent of the high-frequency part of the wave spectrum is within the range -4 to -3. The decay of the high-frequency waves are fastest with depth and hence, the high-frequency tail values observed in the study will be different for different water depths.

Acknowledgments

The authors acknowledge the Earth System Science Organization, Ministry of Earth Sciences, New Delhi for providing the financial support to conduct part of this research. We thank TM Balakrishnan Nair, Head OSISG and Arun Nherakkol, Scientist, INCOIS, Hyderabad and Jai Singh, Technical Assistant, CSIR-NIO for the help during the collection of data. We thank Dr. Bhat and Dr. J L Rathod, Department of Marine Biology, Karnataka University PG Centre, Karwar for providing the logistics required for wave data collection. This work contributes part of the Ph.D. work of the first author. This paper is dedicated to the memory of our esteemed colleague Ashok Kumar, in recognition of his substantial contributions in initiating the long-term wave measurements in the shallow waters around India. We thank the topic editor and both the reviewers for their critical comments and the suggestions which improved the scientific content of the publication. This publication is a NIO contribution.

References

Amrutha, M.M., Sanil Kumar, V., and George, J.: Observations of long-period waves in the nearshore waters of central west coast of India during the fall inter-monsoon period, Ocean Engineering, 131, 244-262, 10.1016/j.oceaneng.2017.01.014, 2017.

Anjali, N.M., and Sanil Kumar, V.: Spectral wave climatology off Ratnagiri - northeast Arabian Sea, Natural Hazards, 82, 1565-1588, 2016.

Badulin, S.I., Babanin, A.V., Zakharov, V.E. and Resio, D.: Weakly turbulent laws of wind-wave growth, Journal of Fluid Mechanics., 591, 339-378, 2007.

Cavaleri, L., Fox-Kemper, B., and Hemer, M.: Wind-waves in the coupled climate sys- tem. Bull. Am. Meteorol. Soc., 93, 1651–1661, 2012.

435 Chakrabarti, S.K.: Handbook of Offshore Engineering, Vol-1, Ocean Engineering Series, Elsevier,
436 p 661, 2005.

437 Chen, G., Chapron, B., Ezraty, R., and Vandemark, D.: A global view of swell and wind-sea
438 climate in the ocean by satellite altimeter and scatterometer. J. Atmospheric and Oceanic
439 Technology., 19(11), 1849-1859, 2002.

440 Datawell.: Datawell Waverider Reference Manual. Datawell BV oceanographic instruments, The
441 Netherlands, Oct. 10, pp.123, 2009.

442 Donelan, M. A.: The effect of swell on the growth of wind waves, Johns Hopkins APL Technical
443 Digest., 8 (1), 18-23, 1987.

444 Donelan, M., Hamilton, H., and Hui, W.H.: Directional spectra of wind-generated waves,
445 Philosophical Transactions of the Royal Society of London A: Mathematical, Physical and
446 Engineering Sciences., 315(1534), 509-562, 1985.

447 Donelan, M.A., Curcic, M., Chen, S.S. and Magnusson, A.K.: Modeling waves and wind stress,
448 Journal of Geophysical Research: Oceans., 117(C11), 2012.

449 Dora, G.U., and Sanil Kumar, V.: Sea state observation in island-sheltered nearshore zone based on
450 in situ intermediate-water wave measurements and NCEP/CFSR wind data, Ocean Dynamics., 65,
451 647-663, 2015.

452 Forristall, G.Z.: Measurements of a saturated range in ocean wave spectra, Journal of Geophysical
453 Research: Oceans., 86(C9), 8075-8084, 1981.Gagnaire-Renou, E., Benoit, M. and Forget, P.: Ocean
454 wave spectrum properties as derived from quasi-exact computations of nonlinear wave-wave
455 interactions, Journal of Geophysical Research: Oceans., 115(C12), 2010.

456 Glejin, J., Sanil Kumar, V., Balakrishnan Nair, T. M., and Singh, J.: Influence of winds on
457 temporally varying short and long period gravity waves in the near shore regions of the eastern
458 Arabian Sea, Ocean Sci., 9, 343–353, doi:10.5194/os-9-343-2013, 2013.

459 Glejin, J., Sanil Kumar, V., Sajiv, P.C., Singh, J., Pednekar, P., Ashok Kumar, K., Dora, G.U., and
460 Gowthaman, R.: Variations in swells along eastern Arabian Sea during the summer monsoon, Open
461 J. Mar. Sci., 2 (2), 43–50, 2012.

462 Glejin, J., Sanil Kumar, V., Amrutha, M.M. and Singh J.:Characteristics of long-period swells
463 measured in the in the near shore regions of eastern Arabian Sea, Int. J. Naval Architecture and
464 Ocean Engineering, 8, 312-319, 2016.

465 Gunson, J., and Symonds, G.: Spectral Evolution of Nearshore Wave Energy during a Sea-Breeze
466 Cycle, J. Phys. Oceanogr., 44(12), 3195-3208, 2014.

467 Harish, C. M., and Baba, M.: On spectral and statistical characteristics of shallow water waves,
468 Ocean Eng., 13(3), 239-248, 1986.

469 Hasselmann, K., Barnett, T.P., Bouws, F., Carlson, H., Cartwright, D.E., Enke, K., Ewing J.A.,
470 Gienapp, H., Hasselmann, D.E., Krusemann, P., Meerburg, A., Muller, P., Olbers, D.J., Richter, K.,
471 Sell, W., and Walden, H.: Measurements of wind-wave growth and swell decay during the Joint
472 North Sea Wave Project (JONSWAP), Deutches Hydrographisches Institut., A8 (12), 95, 1973.

473 Hwang, P.A., Garcia-Nava, H., and Ocampo-Torres, F.J.: Dimensionally Consistent Similarity
474 Relation of Ocean Surface Friction Coefficient in Mixed Seas, J. Phys. Oceanogr 41., 1227–1238.
475 2011.

476 Kahma, K.K.: A study of the growth of the wave spectrum with fetch, Journal of Physical
477 Oceanography., 11(11), 1503-1515, 1981.

478 Kalnay, E., Kanamitsu, M., Kistler, R., Collins, W., Deaven, D., Gandin, L., Iredell, M., Saha, S.,
479 White, G., Woollen, J. and Zhu, Y.: The NCEP/NCAR 40-year reanalysis project, Bulletin of the
480 American meteorological Society., 77(3), 437-471, 1996.

481 Kawai, S., Okada, K. and Toba, Y.: Field data support of three-seconds power law andgu* σ− 4-
482 spectral form for growing wind waves, Journal of Oceanography., 33(3), 137-150, 1977.

483 Kitaigordskii, S.A., Krasitskii, V.P. and Zaslavskii, M.M.: On Phillips' theory of equilibrium range
484 in the spectra of wind-generated gravity waves, Journal of Physical Oceanography., 5(3), 410-420,
485 1975.

486 Kuik, A. J., Vledder, G., and Holthuijsen, L.H.: A method for the routine analysis of pitch and roll
487 buoy wave data, J. Phys. Oceanogr., 18, 1020–1034, 1988.

Liu, A.K., Jackson, F.C., Walsh, E.J. and Peng, C.Y.: A case study of wave-current interaction near an oceanic front, Journal of Geophysical Research: Oceans., 94(C11), 16189-16200, 1989.

Long, C.E. and Resio, D.T.: Wind wave spectral observations in currituck sound, north Carolina, Journal of Geophysical Research: Oceans., 112(C5), 2007.

Longuet-Higgins, M.S.: On the joint distribution of the periods and amplitudes of sea waves, J. Geophys. Res.-Oceans., 80, 2688–2694, 1975.

Neetu, S., Shetye Satish., and Chandramohan, P.: Impact of sea breeze on wind-seas off Goa, west coast of India, Journal Earth System Science., 115, 229-234, 2006.

Pierson, W.J., and Moskowitz, L.: A proposed form for fully developed seas based on the similarity theory of S.A.Kitaigorodski, J. Geophys. Res.-Oceans., 69(24), 5181-5190, 1964.

Portilla, J., Ocampo-Torres, F.J., and Monbaliu, J.: Spectral Partitioning and Identification of Wind-sea and Swell, J. Atmospheric and Oceanic Technology., 26, 117-122, 2009.

Ranjha, R., Tjernström, M., Semedo, A., Svensson, G.: Structure and variability of the Oman Coastal Low-Level Jet, Tellus A, 67, 25285, http://dx.doi.org/10.3402/tellusa.v67.2528 , 2015.

Rao, C. P., and Baba, M.: Observed wave characteristics during growth and decay: a case study, Continental Shelf Res., 16(12), 1509-1520, 1996.

Sanilkumar, V., Ashokkumar, K. and Raju, N.S.N.: Wave characteristics off Visakhapatnam coast during a cyclone, Indian Academy of Sciences., 2004.

Sanil Kumar, V., Johnson, G., Dora, G.U., Chempalayil, S.P., Singh, J., and Pednekar, P.: Variations in nearshore waves along Karnataka, west coast of India, J. Earth Systems Science., 121, 393-403, 2012.

Sanil Kumar, V., Anand, N.M., Kumar, K.A., and Mandal, S.: Multipeakedness and groupiness of shallow water waves along Indian coast, J. Coastal Res., 19, 1052-1065, 2003.

Sanil Kumar, V., and Anand, N.M.: Variation in wave direction estimated using first and second order Fourier coefficients, Ocean Eng., 31, 2105–2119, 2004.

513 Sanil Kumar, V. and Anjali Nair, M.: Inter-annual variations in wave spectral characteristics at a
514 location off the central west coast of India, Ann. Geophys., 33, 159–167, doi:10.5194/angeo-33-
515 159-2015, 2015.

516 Sanil Kumar, V., Shanas, P.R., and Dubhashi, K.K.: Shallow water wave spectral characteristics
517 along the eastern Arabian Sea, Natural Hazards, 70, 377–394, 2014.

518 Semedo, A., Sušelj, K., Rutgersson, A., and Sterl, A.: A global view on the wind-sea and swell
519 climate and variability from ERA-40, J. Climate, 24(5), 1461-1479, 2011.

520 Shetye, S.R., Shenoi, S.S.C., Antony, A.K., and Kumar, V.K.: Monthly-mean wind stress along the
521 coast of the north Indian Ocean, J. Earth Syst. Sci., 94, 129–137, doi:10.1007/BF02871945, 1985.

522 Shore Protection Manual., U.S. Army Coastal Engineering Research Center, Department of the
523 Army, Corps of Engineers, U.S. Govt. Printing Office, Washington, DC, USA, vols. 1 and 2, 1984.

524 Siadatmousavi, S.M., Jose, F. and Stone, G.W.: On the importance of high frequency tail in third
525 generation wave models, Coastal Engineering., 60, 248-260, 2012.

526 Toba, Y.: Local balance in the air-sea boundary processes, Journal of Oceanography., 29(5), 209-
527 220, 1973.

528 Toffoli, A., Onorato, M. and Monbaliu, J.: Wave statistics in unimodal and bimodal seas from a
529 second-order model, European Journal of Mechanics B/Fluids, 25, 649–661, 2006.

530 Torsethaugen, K., and Haver, S.: Simplified double peak spectral model for ocean waves, In:
531 Proceeding of the 14th International Offshore and Polar Engineering Conference, 2004.

532 Vethamony, P., Rashmi, R., Samiksha, S.V. and Aboobacker, M.: Recent Studies on Wind Seas
533 and Swells in the Indian Ocean: A Review, International J. Ocean and Climate Systems, 4, 63 - 73,
534 2013.

535 Young, I.R. and Babanin, A.V.: Spectral distribution of energy dissipation of wind-generated
536 waves due to dominant wave breaking, Journal of Physical Oceanography., 36(3), 376-394, 2006.

537 Yuan, Y., and Huang, N.E.: A reappraisal of ocean wave studies, J. Geophys. Res.-Oceans.,
538 117(C11), 2012.

Figure captions

Figure 1. Study area along with the wave measurement location in eastern Arabian Sea

Figure 2. Time series plot of a) significant wave height, b) mean wave period, c) peak wave period and d) mean wave direction e) maximum spectral energy density from 1 January 2011 to 31 December 2015. Thick blue line indicates the monthly average values

Figure 3. Wave roses during 2011-2015 (a) significant wave height and mean wave direction, (b) peak wave period and mean wave direction, (c) percentage of swell, (d) percentage of wind-sea and mean wave direction

Figure 4. Date verses year plot of a) significant wave height b) mean wave direction, c) peak wave period and d) mean wave period

Figure 5. Temporal variation of normalized spectral energy density (top panel) and mean wave direction (bottom panel) with frequency in different years. The value used for normalizing the spectral energy density is presented in Fig. 2e.

Figure 6. Monthly average wave spectra in 2011 to 2015

Figure 7. Wave spectra averaged over a) pre-monsoon (February-May), b) monsoon (June-September), c) post-monsoon (October-January) and d) full year in different years

Figure 8. Monthly average wave direction at different frequencies in different months

Figure 9. Temporal variation of normalized spectral energy density in different months (data from 2011 to 2015 used). The value used for normalizing the spectral energy density is presented in Fig. 2e.

Figure 10. Scatter plot of significant wave height with skewness of the sea surface elevation in different years

Figure 11. Plot of exponent of the high-frequency tail with a) significant wave height, b) mean wave period, c) wind speed, d) inverse wave age, e) u-wind and f) v-wind

Figure 12. Fitted theoretical spectra along with the monthly average wave spectra for different month

566 Table 1. Number of data used in the study in different years along with range of significant wave
567 height and average value
568

Year	Significant wave height (m)		Number of data	%of data
	Range	Average		
2011	0.3-4.4	1.1	17517	99.98
2012	0.3-3.7	1.1	17323	98.61
2013	0.3-3.6	0.9*	14531	82.94
2014	0.3-4.5	1.1	17284	98.65
2015	0.3-5.0	1.1	14772	84.32

569 * average value is estimated excluding the July month data
570
571
572
573
574
575
576 Table 2. Characteristics of waves in different range of significant wave height
577

Significant wave height range	Number (percentage)	Range of Tp (s)	Mean Tp (s)	Range of T_{m02} (s)	Mean T_{m02} (s)
$H_{m0} < 1$ m	52062 (63.94)	2.6-22.2	12.2	2.7-10.5	4.9
$1 \leq H_{m0} < 2$ m	18297 (22.47)	3.6-22.2	10.5	3.4-10.7	5.7
$2 \leq H_{m0} < 3$ m	9839 (12.08)	6.2-18.0	10.8	5.0-8.9	6.5
$3 \leq H_{m0} < 4$ m	1096 (1.35)	10.0-14.3	11.8	6.1-9.1	7.2
$4 \text{ m} \leq H_{m0}$	133 (0.16)	10.5-14.3	12.6	7.2-9.3	7.8

578
579
580
581
582
583
584 Table 3. Average wave parameters and number of data in different spectral peak frequencies
585

Frequency (f_p) range (Hz)	Number of data and %	H_{m0} (m)	T_{m02} (s)	Peak wave period (s)
$0.04 < f_p \leq 0.05$	318 (0.39)	0.73	5.24	20.19
$0.05 < f_p \leq 0.06$	5341 (6.56)	0.82	5.48	17.16
$0.06 < f_p \leq 0.07$	14764 (18.13)	0.75	5.22	14.73
$0.07 < f_p \leq 0.08$	18221 (22.38)	0.80	5.05	12.96
$0.08 < f_p \leq 0.10$	25364 (31.15)	1.55	5.76	10.88
$0.10 < f_p \leq 0.15$	9459 (11.62)	1.25	5.35	8.07
$0.15 < f_p \leq 0.20$	6355 (7.80)	0.76	4.43	5.72
$0.20 < f_p \leq 0.30$	1487 (1.83)	0.78	3.86	4.36
$0.30 < f_p \leq 0.50$	118 (0.14)	0.66	3.22	3.09

586

Table 4. Exponent of the high-frequency tail of the monthly average wave spectra in different years

Months	Exponent of the high-frequency tail					
	2011	2012	2013	2014	2015	2011-2015
January	-2.08	-2.93	-2.97	-2.72	-2.81	-2.72
February	-2.41	-3.02	-2.74	-2.99	-3.06	-2.85
March	-2.75	-2.91	-2.82	-2.76	No data	-2.81
April	-2.56	-2.74	-2.64	-2.71	-2.19	-2.60
May	-2.59	-2.67	-2.63	-2.42	-2.51	-2.56
June	-3.64	-3.53	-3.55	-3.82	-3.58	-3.55
July	-3.76	-3.55	No data	-3.82	-3.63	-3.70
August	-3.63	-3.58	-3.40	-3.52	-3.65	-3.58
September	-3.41	-3.44	-3.16	-3.38	-3.00	-3.30
October	-2.02	-2.77	-3.03	-2.52	-2.61	-2.68
November	-1.78	-2.43	-1.77	-1.55	-1.65	-1.84
December	-1.69	-2.23	-1.95	-2.06	-1.79	-1.94

Table 5. Exponent of the high-frequency tail of the average wave spectra in different wave height ranges

Range of H_{m0} (m)	Exponent of the high-frequency tail
0-1	-2.44
1-2	-3.26
2-3	-3.67
3-4	-4.21
4-5	-4.21

603 Table 6. Parameters of the fitted wave spectrum in different years
604
605

Year		JONSWAP spectrum		Donelan spectrum	
		α	ϒ	α	ϒ
2011	June	0.0013	2.2	0.0028	2.0
	July	0.0016	1.5	0.0021	1.7
	August	0.0013	1.8	0.0029	1.7
	September	0.0004	2.3	0.0021	1.6
2012	June	0.0015	1.6	0.0029	2.0
	July	0.0010	2.1	0.0031	1.9
	August	0.0009	2.2	0.0032	1.7
	September	0.0006	2.0	0.0024	1.8
2013	June	0.0006	3.3	0.0030	1.9
	July	No data			
	August	0.0012	1.1	0.0038	1.4
	September	0.0005	1.9	0.0042	1.4
2014	June	0.0010	1.1	0.0010	1.6
	July	0.0006	2.5	0.0019	1.2
	August	0.0006	1.5	0.0021	1.2
	September	0.0011	1.1	0.0032	1.4
2015	June	0.0011	1.4	0.0023	1.8
	July	0.0011	1.9	0.0024	1.8
	August	0.0008	1.8	0.0024	1.4
	September	0.0006	1.3	0.0043	1.6

606
607

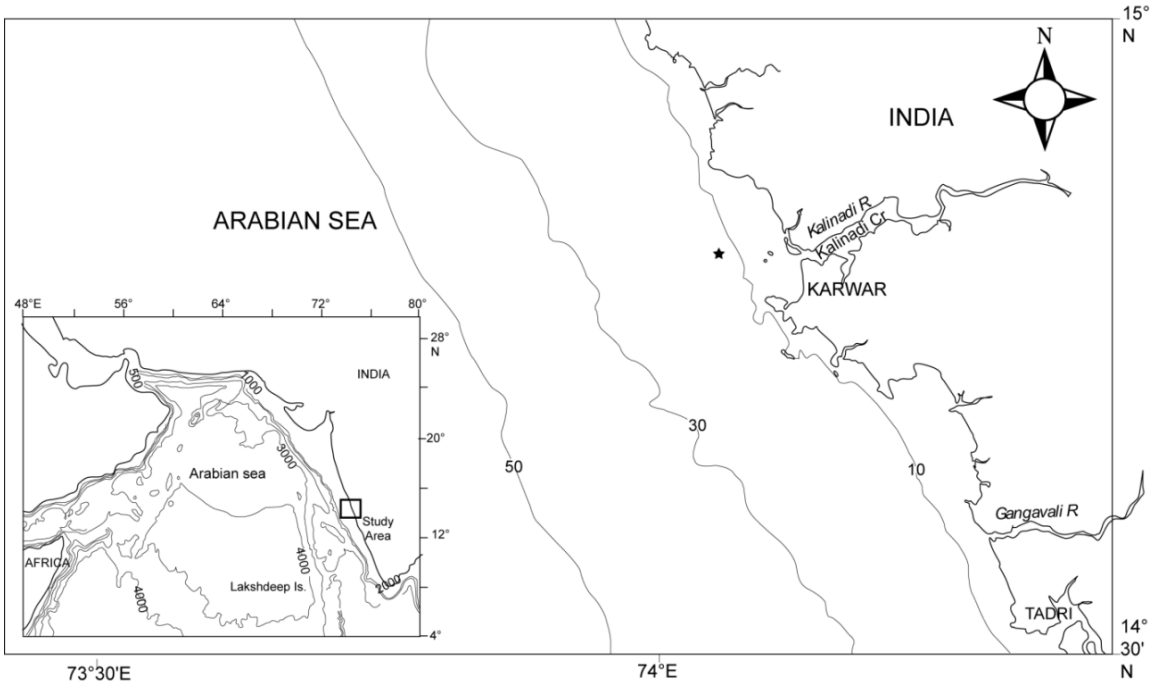

Figure 1. Study area along with the wave measurement location in eastern Arabian Sea

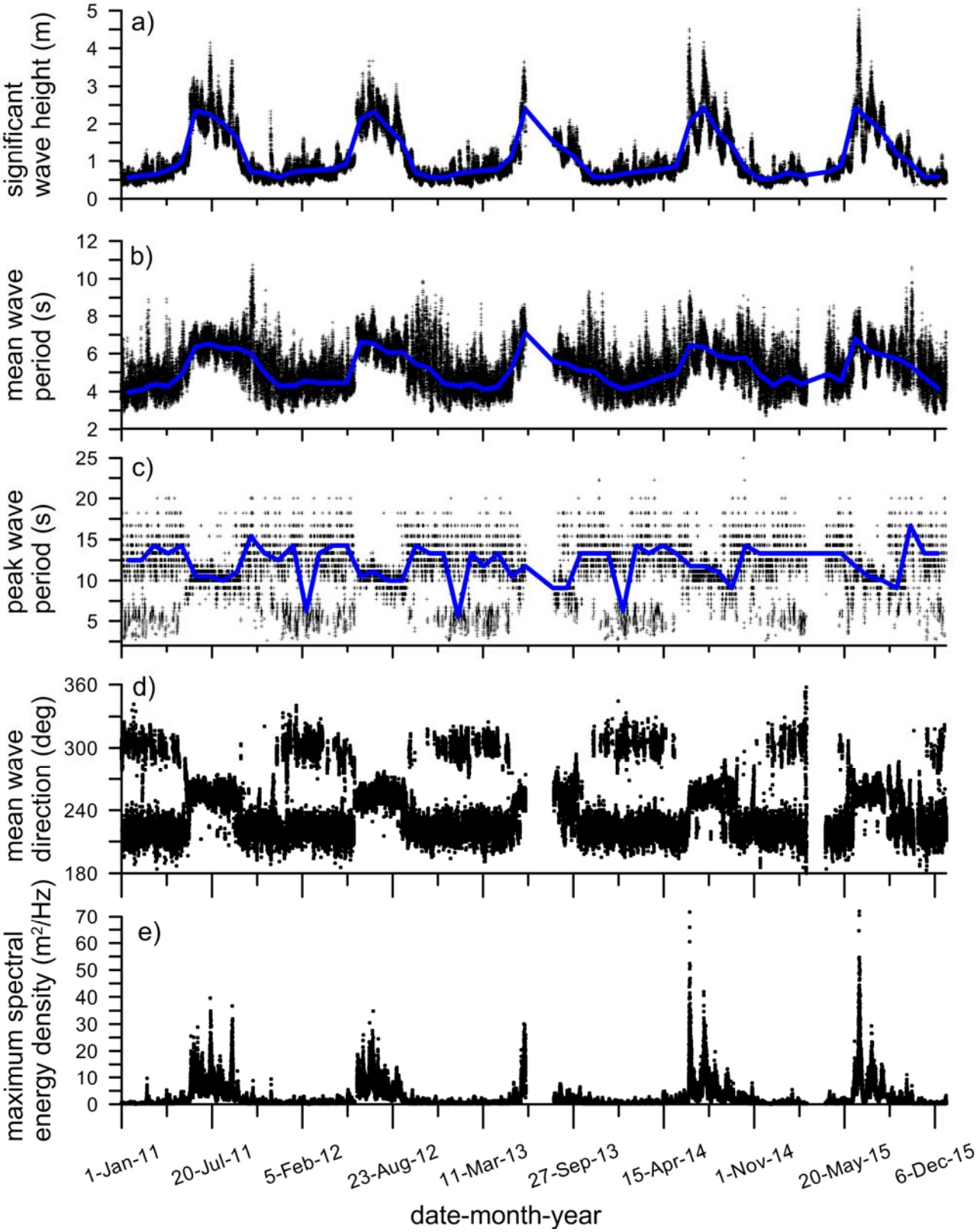

Figure 2. Time series plot of a) significant wave height, b) mean wave period, c) peak wave period and d) mean wave direction e) maximum spectral energy density from 1 January 2011 to 31 December 2015. Thick blue line indicates the monthly average values

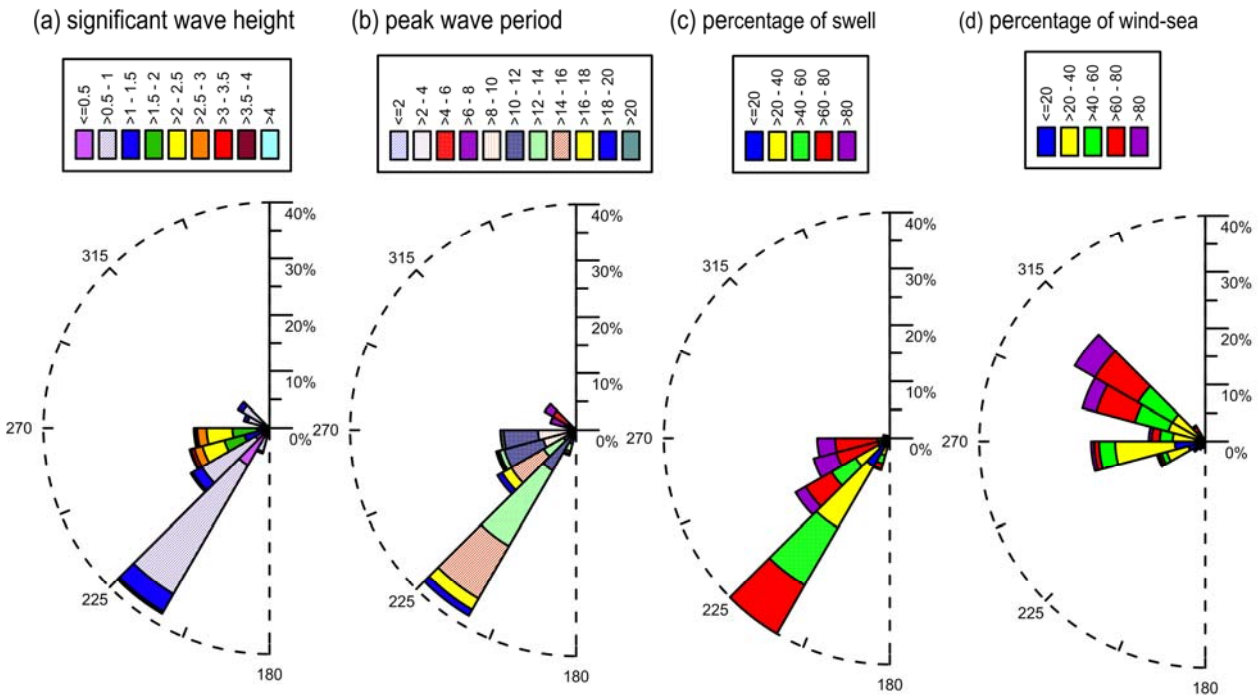

Figure 3. Wave roses during 2011-2015 (a) significant wave height and mean wave direction, (b) peak wave period and mean wave direction, (c) percentage of swell, (d) percentage of wind-sea and mean wave direction

620
621

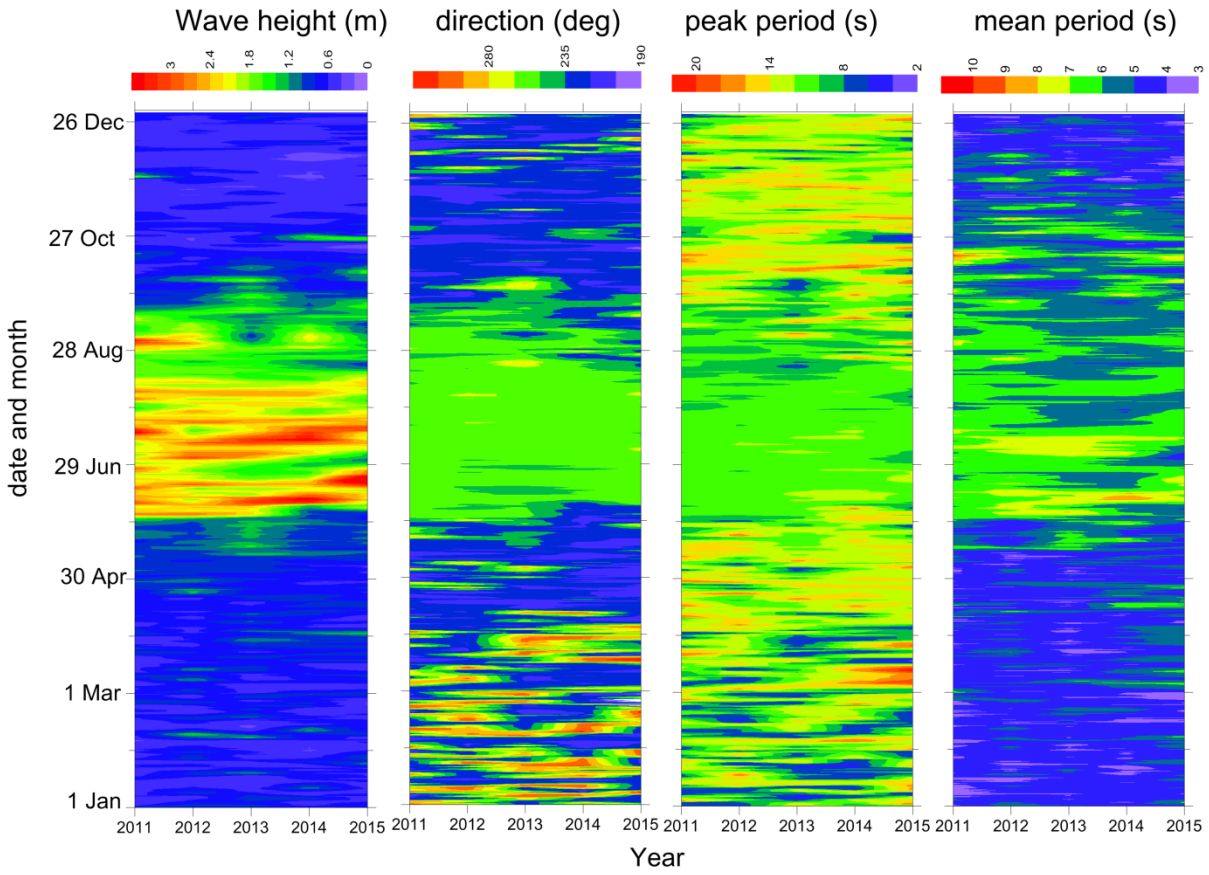

622
623 Figure 4. Date verses year plots of a) significant wave height b) mean wave direction, c) peak wave
624 period and d) mean wave period.
625

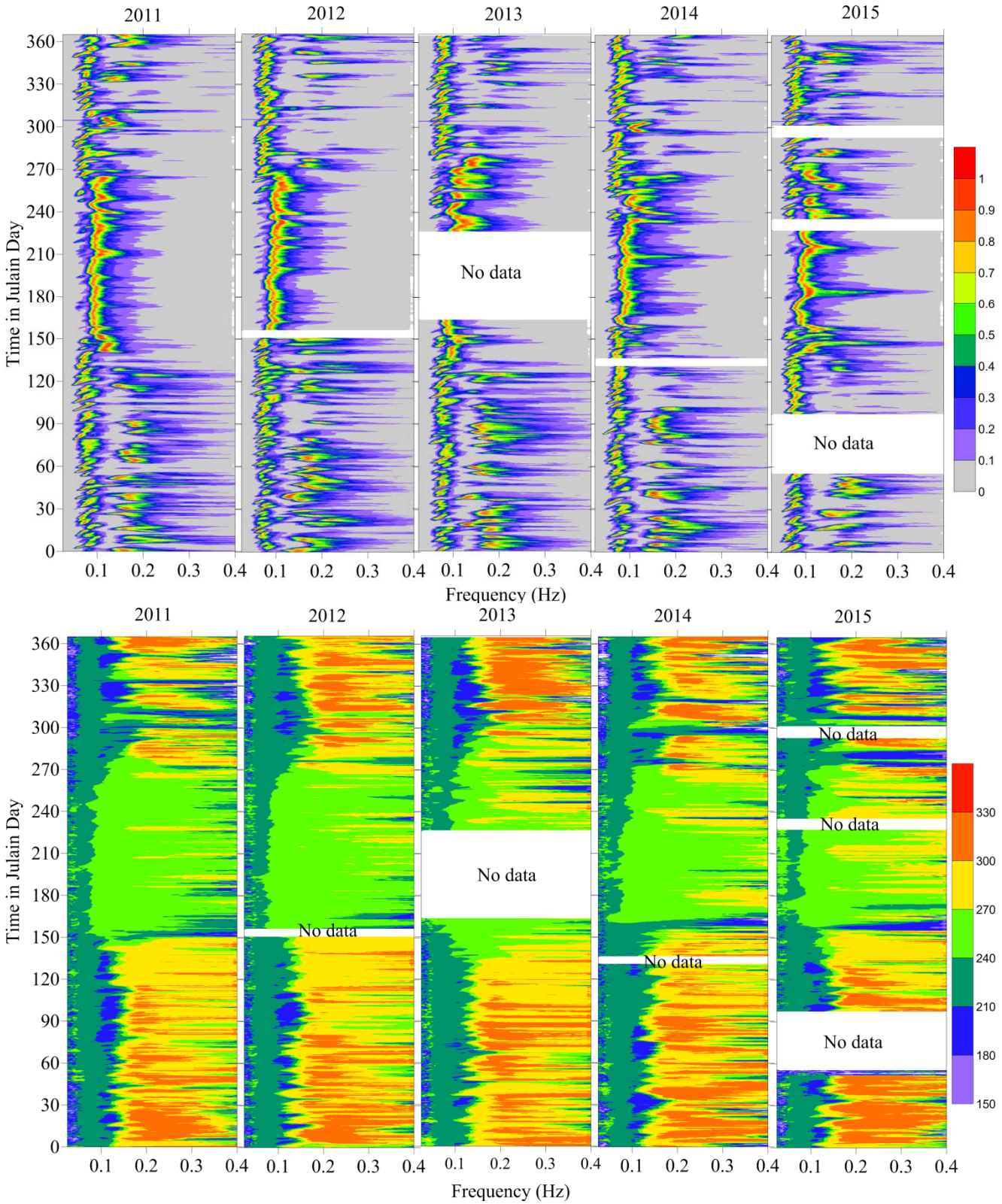

Figure 5. Temporal variation of normalized spectral energy density (top panel) and mean wave direction (bottom panel) with frequency in different years. The value used for normalizing the spectral energy density is presented in Fig. 2e.

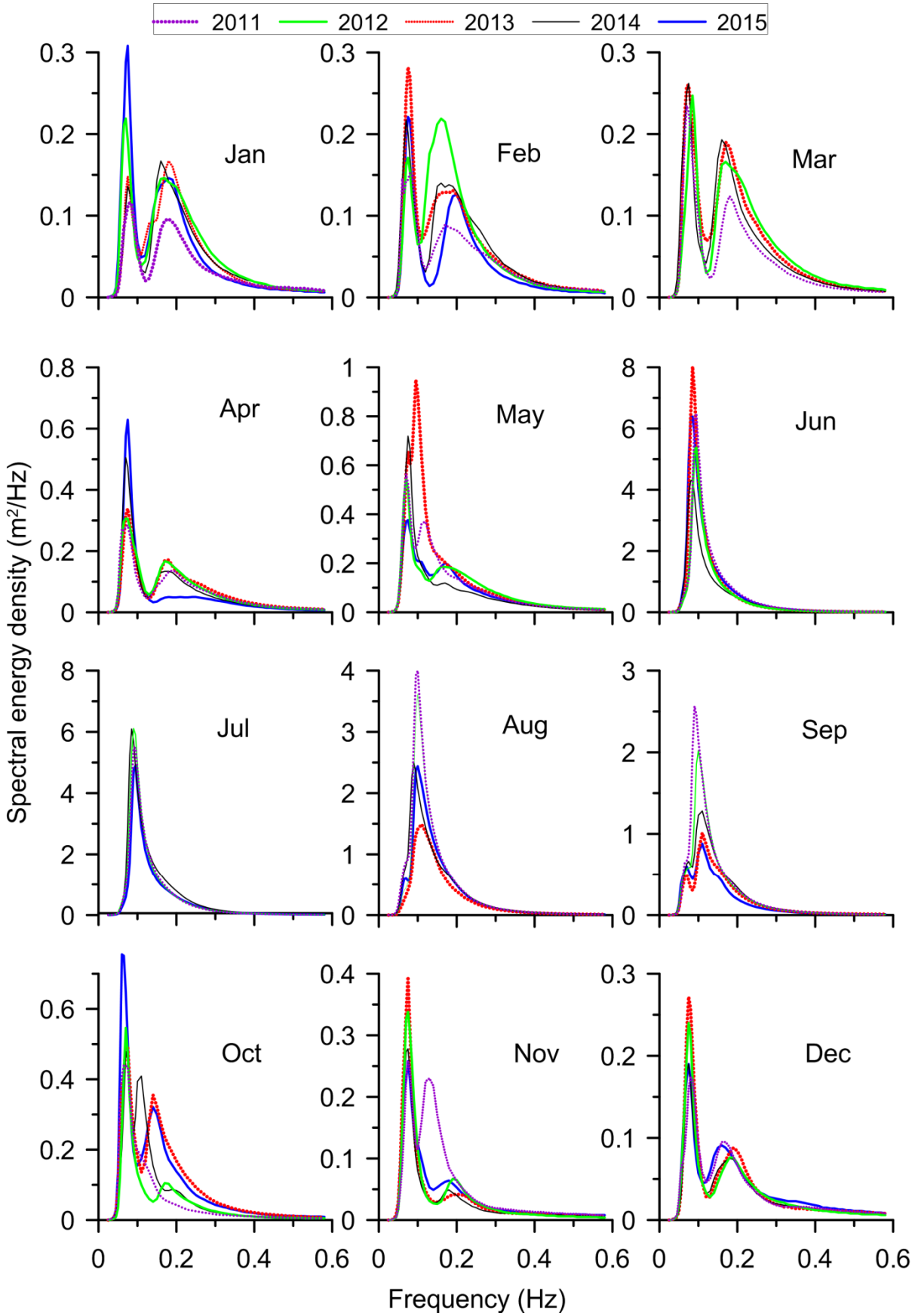

633
634 Figure 6. Monthly average wave spectra in 2011 to 2015

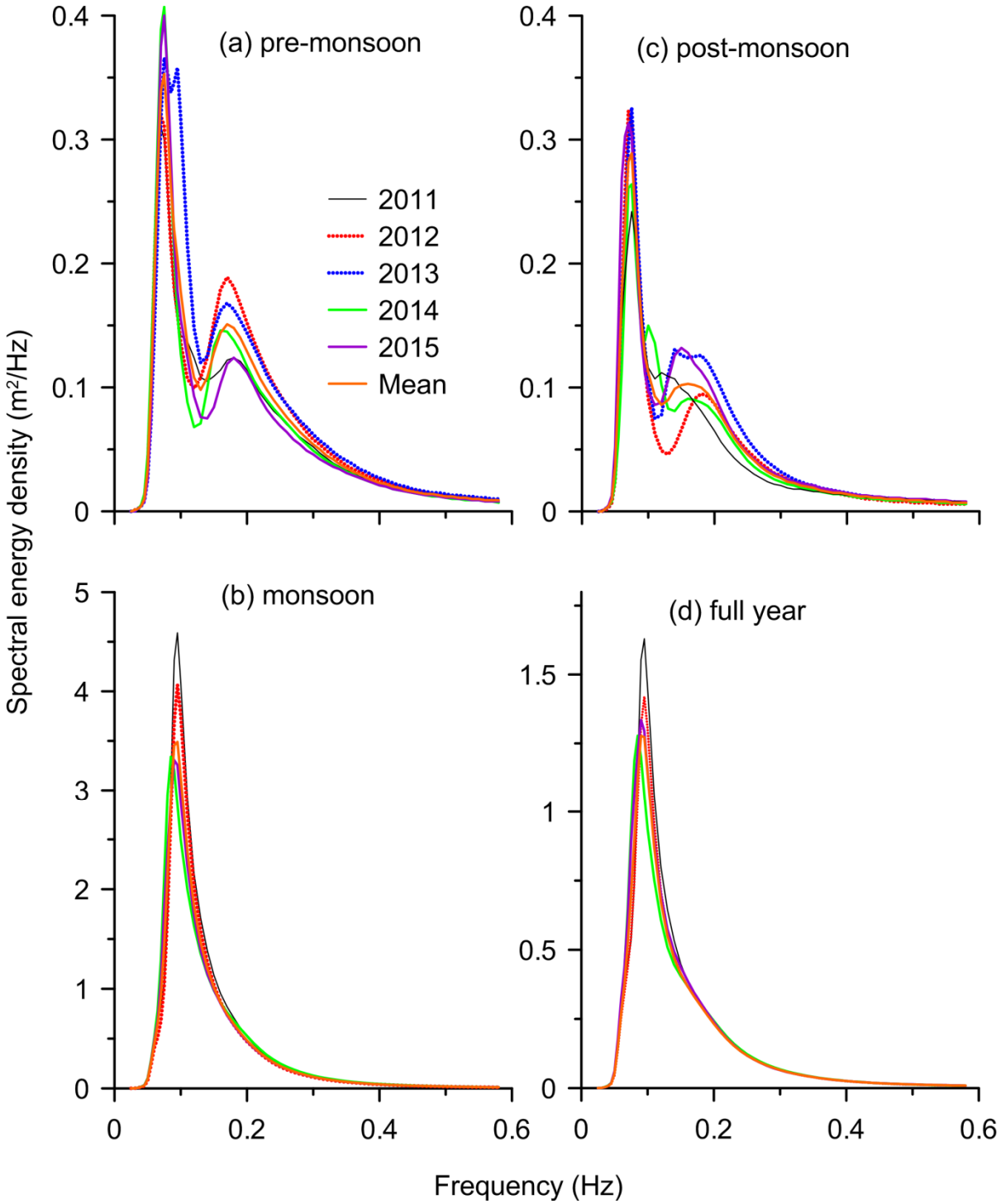

Figure 7. Wave spectra averaged over a) pre-monsoon (February-May), b) monsoon (June-September), c) post-monsoon (October-January) and d) full year in different years

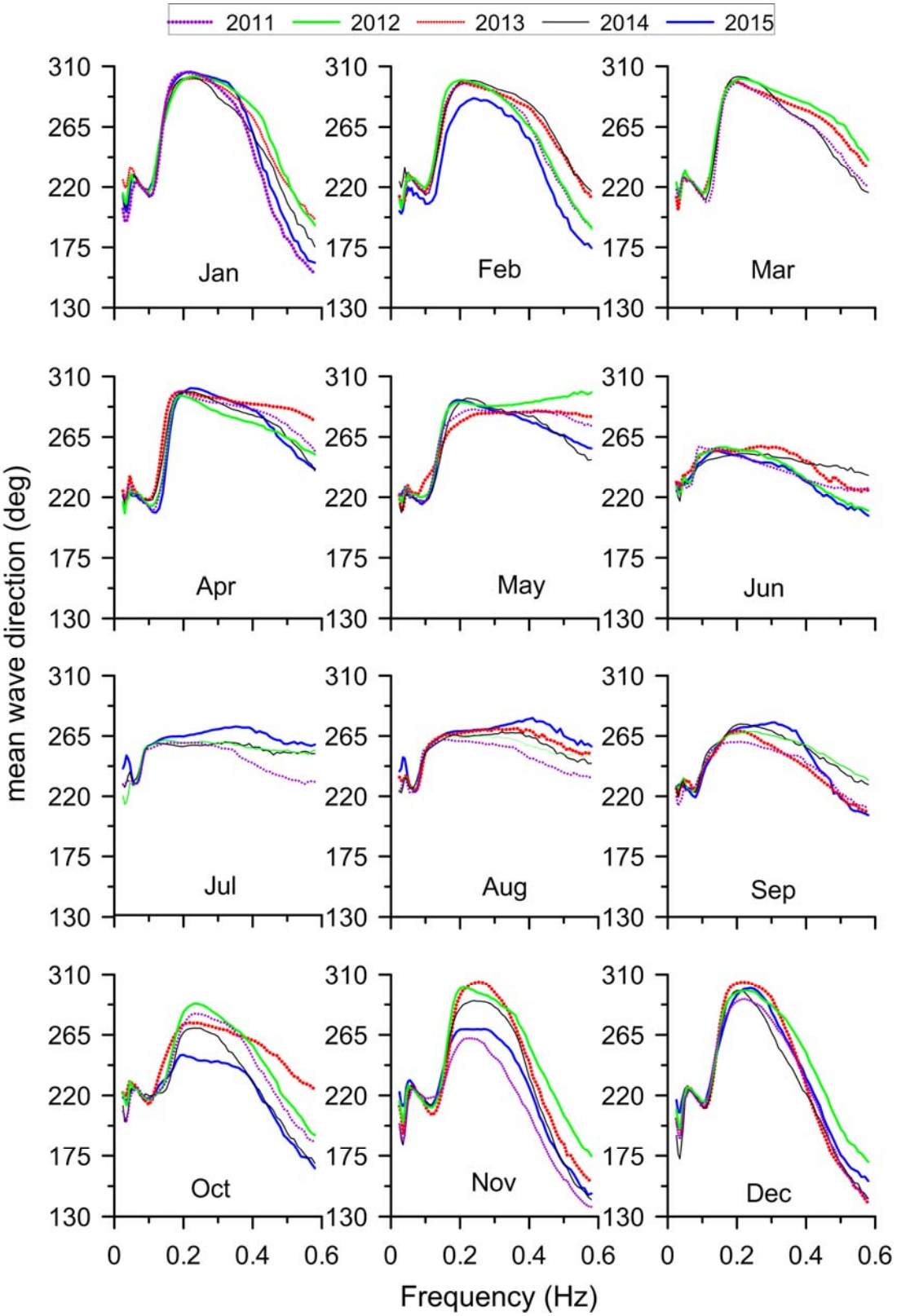

Figure 8. Monthly average wave direction at different frequencies in different months

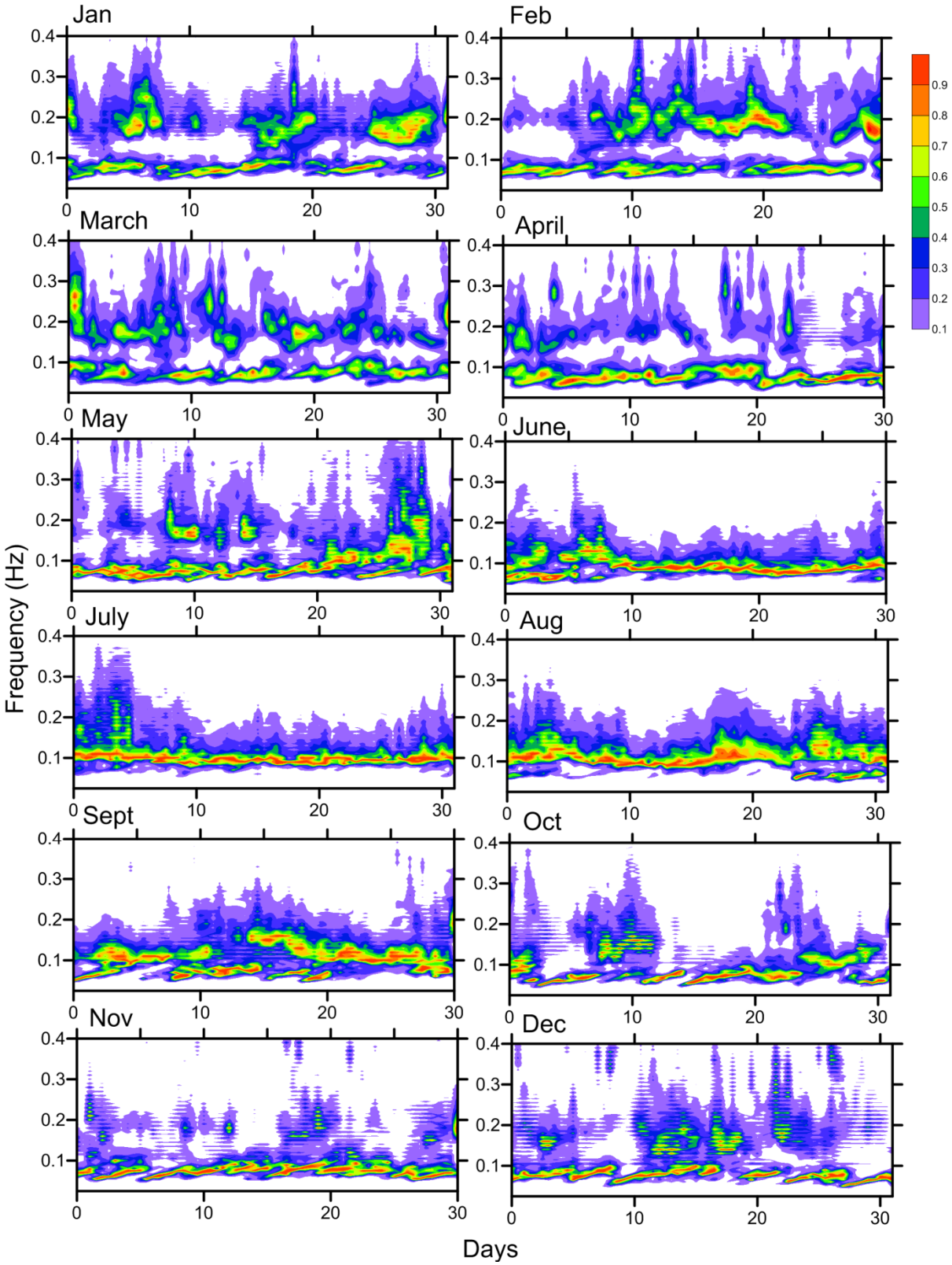

644
645 Figure 9. Temporal variation of normalized spectral energy density in different months (data from
646 2011 to 2015 used). The value used for normalizing the spectral energy density is presented in Fig.
647 2e.
648

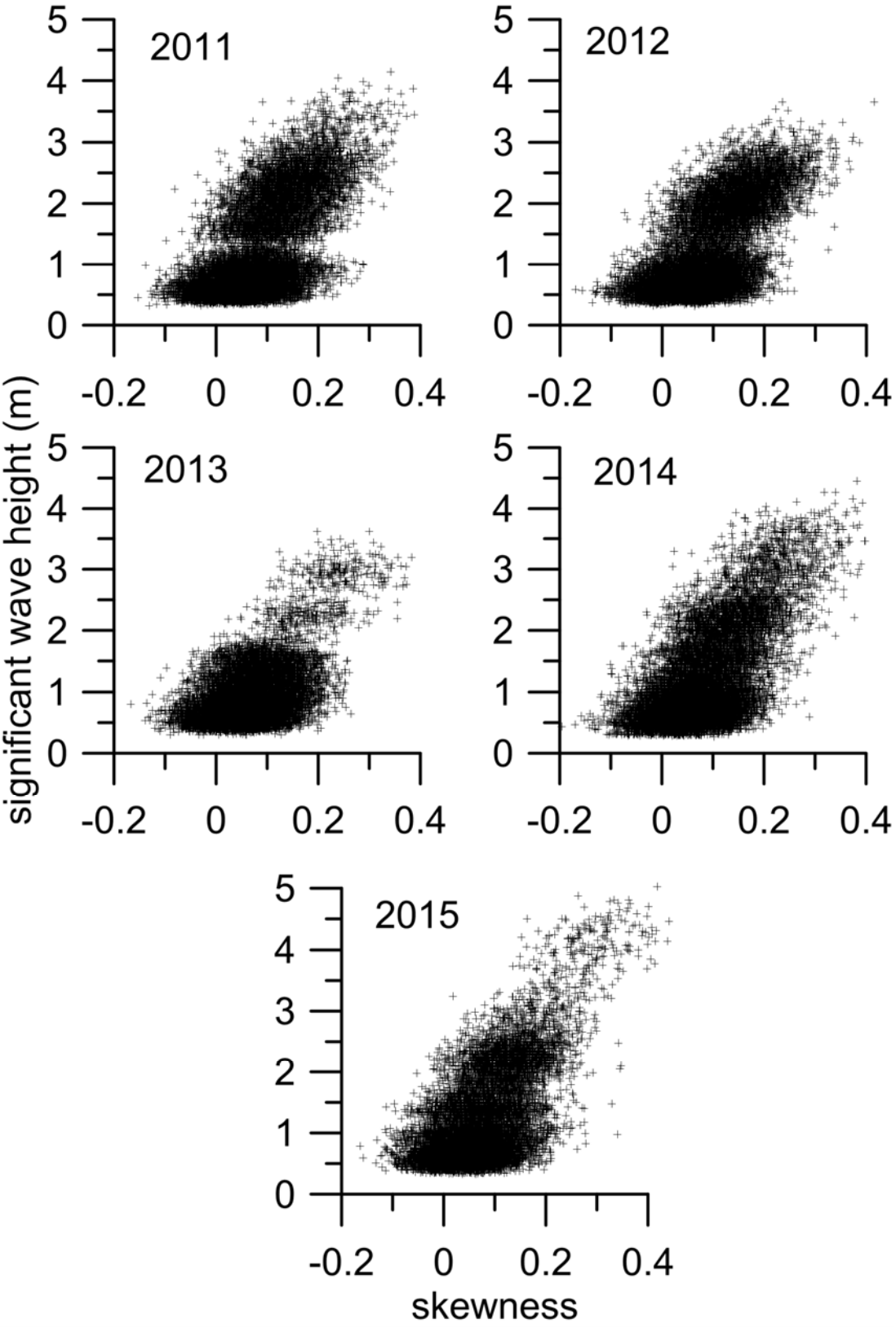

649
650
651 Figure 10. Scatter plot of significant wave height with skewness of the sea surface elevation in
652 different years

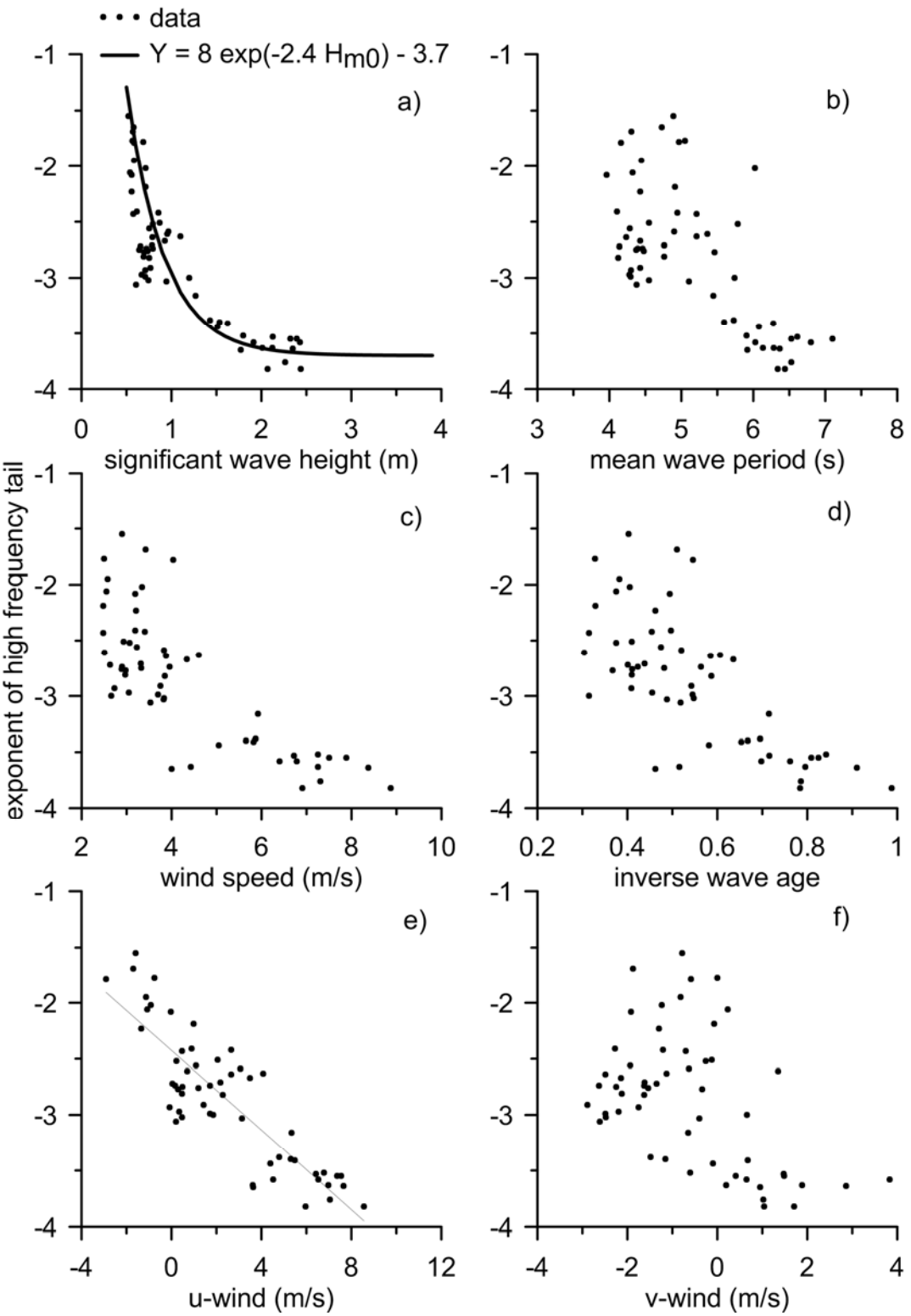

Figure 11. Plot of exponent of the high-frequency tail with a) significant wave height b) mean wave period, c) wind speed, d) inverse wave age, e) u-wind and f) v-wind

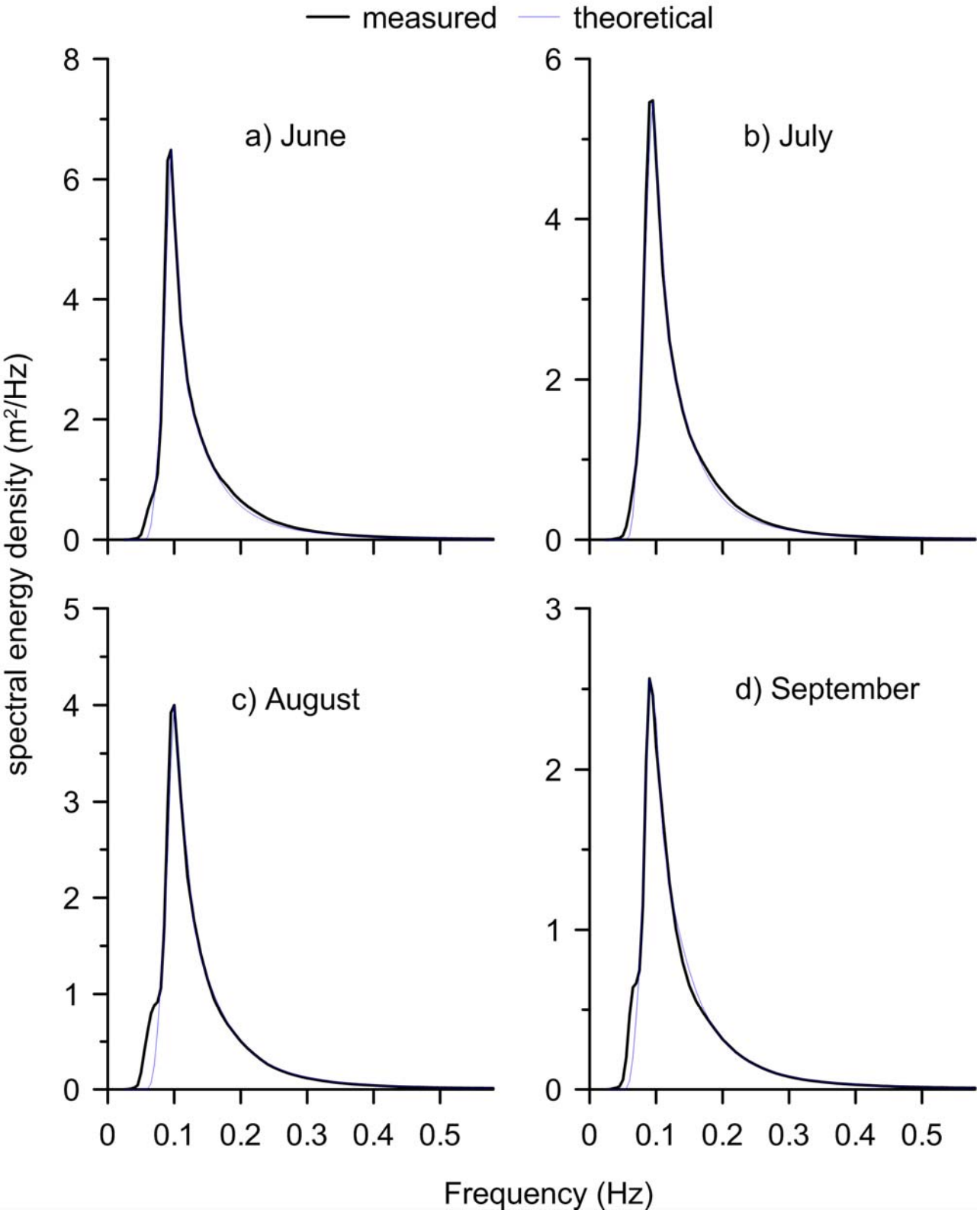

656
657 Figure 12. Fitted theoretical spectra along with the monthly average wave spectra for a) June, b)
658 July, c) August and d) September